The Journal of Chemical Physics

Monitoring damage of self-assembled monolayers using metastable excited helium atoms.

Georgios Stratis,[1, a)] Jordan D. Zesch,[1] Henry S. Pan,[2] Lauren J. Webb,[3] and Mark G. Raizen[1]

[1)]*Department of Physics, University of Texas at Austin, Austin, Texas 78712, USA*

[2)]*McKetta Department of Chemical Engineering,University of Texas at Austin, Austin, Texas 78712, USA*

[3)]*Department of Chemistry, University of Texas at Austin, Austin, Texas 78712, USA*

(Dated: December 22, 2020)

The breaking of molecular bonds during exposure to ionizing radiation and electron beams creates irreversible damage in the molecular structure. In some cases, such as lithography, controlled damage of a molecular resist is a desirable process and is the basis for the entire semiconductor industry. In other cases, like environmental exposure or probing of molecular structure, the induced damage is a major problem that has limited advances in science and technology. We report here the use of an in-situ probe that is minimally invasive to detect real-time damage induced in organic materials. Specifically, we use metastable excited helium atoms in the $^3S_1$ state to characterize the damage caused by a low energy electron beam $\sim$30 eV on an organic self-assembled monolayer of 11-bromo-1-undecanethiol (BrUDT) on a gold substrate. We were able to monitor the damage caused by the electron beam without introducing any additional observed damage by the probing metastable atoms.

[a)]stratis@utexas.edu

I. INTRODUCTION

The damage of molecular bonds by external agents is a well-studied phenomenon that is ubiquitous in nature, such as DNA damage by ionizing radiation which can lead to cancer.[1,2] It is employed in a controlled manner for important technological applications such as lithography for the semiconductor industry.[3,4] Damage can occur by various mechanisms, such as exposure to electrons[5] or short-wavelength photons.[6] Determination of the structure of individual molecules, specifically proteins, is a long-standing goal of science and technology. Indeed, the required resolution is already in hand with modern electron microscopes, but organic materials are severely damaged by electron beams, limiting the applicability of such probes.[7] New approaches, such as cryogenic electron microscopy,[8] are making impressive advances, while understanding and controlling the mechanisms for damage remain an important challenge. An ideal platform for performing these studies are self-assembled monolayers (SAMs), organic films that can be readily grown on substrates, and are amenable to a range of analytic probes. In this paper, we focus on SAMs that are chemisorbed by a sulfur-substrate bond onto substrates such as bare metal,[9] metal-oxide surfaces,[10] semiconductors,[11] and graphene.[12] These films are typically 1 nm to 3 nm, simple to fabricate, chemically tunable, and are stable for days under ambient conditions.[13] Given these favorable characteristics, SAMs have been used in a plethora of different surface applications, ranging from electron beam lithography[14,15] to influencing the secondary structure of biomolecules,[16] as well as sensing applications.[17,18] In the work presented here, SAMs formed with alkanethiols on bare-gold substrate were chosen because their orderly, crystalline structures have been well-established through a variety of surface characterization techniques,[19–22] making any induced disorder caused by irradiation damage easy to detect. Previous work has shown that damage to organic samples[1,23] can be caused by irradiation during ultraviolet (UV)[24] and X-ray spectroscopy (XPS),[25,26] as well as by the electron beam in scanning electron microscopy (SEM) and transmission electron microscopy (TEM).[7] It has been established that damage on SAMs manifest as bond dissociation[27,28] as well as cross-linking.[14] Interestingly, the induced damage has been attributed to photoelectrons and secondary electrons when the samples are exposed to x-rays.[25] In the case where the samples are being directly probed or exposed to an electron beam, the beam's energy plays an important role in the damage caused to SAMs.[29–31] In the above experiments the samples were significantly damaged by the probing beam itself, leading to additional damage to the sample. To address this issue, we utilize metastable atom electron spectroscopy

(MAES) in order to monitor the damage induced by an electron beam on a self-assembled monolayer, and demonstrate real-time probing of the surface. The surface sensitivity of MAES allows one to probe only the changes taking place at the top-most layer of a sample without getting contributions from the underlying substrate. This new use of an analytic tool will enable the delineation of the role of the underlying substrate on damage, and potentially provide new approaches towards non-destructive probing of organic molecules. MAES has been used in the past to determine the energy density of states for alkanethiol SAM[32] as well as to study the effect of ion sputtering.[20]

II. ELECTRON EMISSION VIA METASTABLE ATOM DE-EXCITATION

Metastable atoms are atoms in excited states with long lifetime relative to the duration of the experiment. In our experiment we are using helium atoms excited in the triplet $^3S_1$ state which is $\sim$19.8 eV above the ground state and has a lifetime of $\sim$7870 s.[33] Metastable atoms de-excite almost with unit probability upon impact with a surface[34] via an Auger process[35,36] causing a subsequent electron emission from the sample. Depending on the material and the metastable atom used, there are different channels by which a metastable atom de-excites.[35–40] The location of the sample's Fermi energy with respect to the continuum, the location of the metastable energy with respect to the continuum, and the unoccupied energy bands of the material determine which of the mechanisms can take place. In all of the different de-excitation mechanisms the electron emission is a result of electron tunneling between the incoming metastable atom and the surface of the sample. As a consequence, metastable atoms probe only the surface-most layer of a sample[35,36] since they do not interact with its bulk. Even though virtually all the metastable atoms de-excite, this does not translate to an equal amount of emitted electrons.[41]

In materials where all the energy levels below the metastable state are occupied, the electron emission is due to the Auger de-excitation (AD) process. These materials are mainly insulators, where the metastable level falls in the insulator's band gap, and low work function metals, where the Fermi energy is above the metastable energy level. In these scenarios, as the metastable atom approaches the surface, a surface electron tunnels into the atom's ground state causing the atom's outermost electron to be emitted (fig. 1). During the AD process the total energy of the system is conserved. Assuming negligible change in the kinetic energy of the impinging atom, the emitted electron's kinetic energy needs to obey

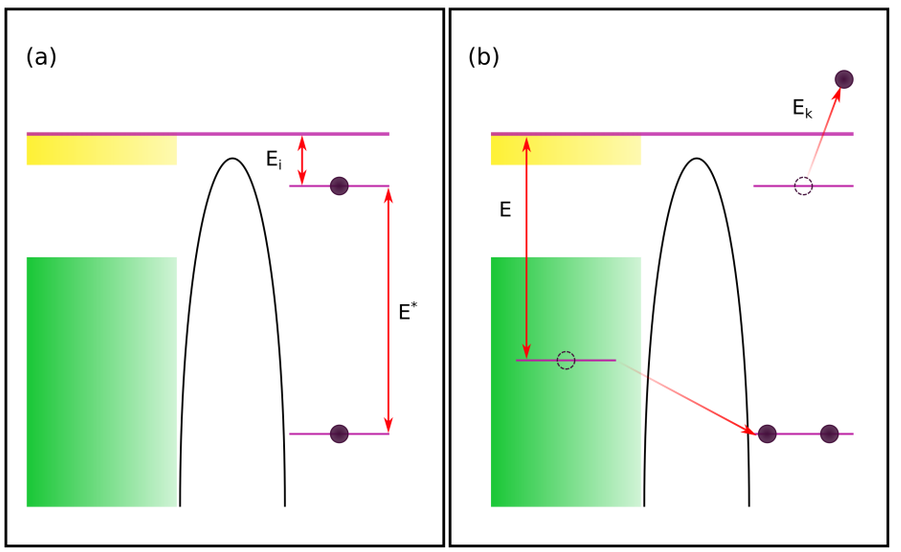

Figure 1. In panel (a), we illustrate the atom's energy levels as well as the material's when the atom is far away from the material's surface. The yellow band indicates the unoccupied energy levels of the material and the green band indicates the occupied energy levels. E^* is the energy difference between the atom's metastable energy level and its ground energy level. E_i is the energy difference between the energy continuum and the metastable energy level and it stands for the energy needed to ionize the metastable atom. In panel (b), we illustrate the Auger de-excitation (AD) process which takes place once the atom is close enough ($<$10 Å) to the material's surface. An electron occupying an energy level with energy E with respect to the continuum tunnels to the ground state of the impinging atom. This leads to one of the atom's electrons to be emitted with kinetic energy E_k. By collecting the emitted electrons and measuring their kinetic energy we can collect information about the material's energy levels.

$$\begin{aligned} E_k + E_i - E^* &= E_i - E \\ \implies E_k &= E^* - E\,. \end{aligned} \tag{1}$$

In eq. (1) E_k stands for the kinetic energy of the emitted electron, E^* is the energy difference between the metastable and the ground state of the incoming atom, E_i is the ionization energy of

the metastable atom, and E is the energy level that the surface electron occupied before it was emitted.

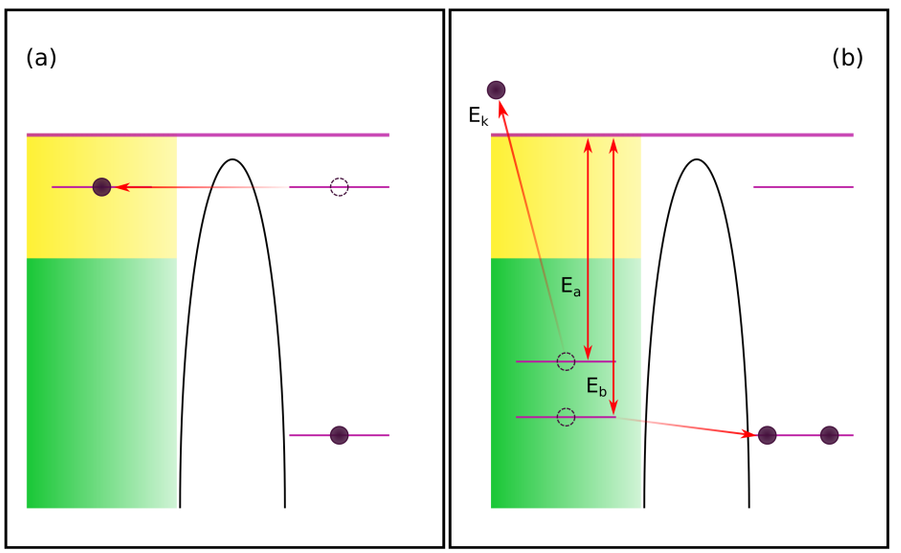

Figure 2. For materials with a Fermi energy below the metastable state, the impinging metastable atom can also de-excite via a two-stage process besides the Auger de-excitation process. Panel (a) illustrates the resonance ionization (RI) process which is the first stage of the de-excitation process. In this stage, the electron occupying the outermost orbital of the metastable atom tunnels into an unoccupied energy level of the material under investigation. This causes the ionization of the metastable atom. Panel (b) illustrates the Auger neutralization (AN) process which is the second stage of the de-excitation process. In this stage, a surface electron tunnels into the ground state of the newly created ion; thus neutralizing it. Finally, a second surface electron gets emitted. E_k indicates the kinetic energy of the emitted electron, E_a is the energy level the emitted electron occupied before its emission, E_b is the energy level the tunneled electron occupied before the tunneling took place.

When the Fermi energy of the sample is lower than the metastable level, the metastable atom can also de-excite following a two-stage process (fig. 2). In the first stage, the electron occupying the outermost shell of the metastable atom tunnels into an unoccupied energy level of the material

causing the metastable atom's ionization. Hence the first stage is referred to as a resonance ionization (RI) process. As the newly created ion gets even closer to the surface, a surface electron tunnels in the ground state of the ion, causing its neutralization, and a second surface electron is emitted. Thus the second stage is referred to as an Auger neutralization (AN) process. Similarly with the AD process, the total energy of the system is conserved. Assuming negligible change in the kinetic energy of the impinging atom, the emitted electron's kinetic energy needs to obey

$$\begin{aligned} E_k &= E^* - E_a - E_b, \\ E_a &= \phi + \Delta - \varepsilon, \\ E_b &= \phi + \Delta + \varepsilon, \\ \implies E_k &= E_i - 2\phi - 2\Delta. \end{aligned} \tag{2}$$

.

In eq. (2) E_k stands for the kinetic energy of the emitted electron, E^* is the energy difference between the metastable and ground states of the incoming atom, E_i is the ionization energy of the neutral atom, E_a is the energy level that the surface electron occupied before it was emitted, E_b is the energy level of the surface electron that ended up tunneling into the ion, ϕ is the work function of the sample, Δ is the average energy of E_a and E_b, and ε is the energy difference from E_a and E_b to Δ. This is the main de-excitation channel when metastable atoms encounter most metals. It should be noted that the AD process also takes place at the same time, although it is less prevalent.

III. METHODS

The experimental procedures include making SAMs, diagnosing quality using Fourier transform infrared (FTIR) spectroscopy, taking spectra using MAES, and damaging the sample using an electron beam. SAMs were fabricated based on the procedures used in prior work.[42] SAMs were made on a substrate of gold-coated silicon wafers (Ted Pella). The 50 nm gold layer was adhered to a $\langle 111 \rangle$ silicon wafer by a 5 nm chromium layer. The wafer was covered with clean-room rated silicon wafer tape and cut into 10 mm $\times$ 10 mm substrates using a programmable wafer dicing saw. The tape was removed from each substrate and any residue was removed through sonication in acetone for 10 minutes. Substrates were then cleaned by immersion for 1 minute in piranha solution (1:3 30% hydrogen peroxide/concentrated sulfuric acid; ***caution****: explosive in the presence of organic contaminants*), rinsed in ultra-pure water, then rinsed in anhydrous ethanol.

Substrates were completely dried under a stream of N_2. Subsequently, substrates were annealed with a low pressure hydrogen flame ($\approx$10 psi) which was passed over the samples for 10 rounds of 25 s each, with 5 s cooling intervals between rounds. The SAM solutions were made with the desired thiol diluted in anhydrous ethanol to a concentration of 1 mM. We made samples using 11-bromo-1-undecanethiol (BrUDT) (Sigma Aldrich, 99%) and 1-dodecanethiol (DDT) (Sigma Aldrich, $\geq$ 96%). The substrates were immersed in 4 mL of solution for 24 hours in the dark to ensure highly packed thiol surfaces.[43] The samples were then removed, rinsed in water then anhydrous ethanol, and dried under a stream of N_2. Samples were checked for well-ordered SAMs using FTIR spectroscopy (Bruker, VERTEX 80). Spectra were calculated as $-\log(R/R_0)$, where R was the reflectivity of a SAM on the substrate and R_0 was the reflectivity of the gold substrate. The FTIR spectra for a BrUDT and a DDT SAM are provided in fig. 3. We are using the location of the peaks in the CH_2 stretching region (2919, 2851 cm^{-1}) as reported in reference[19] to determine the quality of our SAM. The BrUDT sample had peaks at 2918 and 2847 cm^{-1} and the DDT sample had peaks at 2917 and 2847 cm^{-1} which indicates that in both samples we had well-ordered SAMs. Moreover, the DDT sample exhibited peaks at 2964 and 2878 cm^{-1} which correspond to the CH_3 stretching region (2965, 2879 cm^{-1})[19]. These peaks were absent in the BrUDT sample due to BrUDT not having a CH_3 group.

The experimental apparatus consisted of two vacuum chambers and is shown in fig. 4. During the experiment, the pressure in the vacuum chamber where the metastable atoms were produced was at $\sim 10^{-5}$ Torr. Due to the skimmer's small opening (3 mm), there was differential pumping between the two vacuum chambers and the second chamber, where the sample was located, was at $\sim 10^{-9}$ Torr. The atomic beam was generated by a supersonic pulsed nozzle fed with ground state helium at a pressure of 400 *psi*. The nozzle operated at a 4 Hz repetition rate with 32.5 µs duration pulses. A pair of electrodes (discharge plates) in front of the nozzle created an electrical discharge which excited a fraction of the helium atoms to the desired 2^3S_1 metastable state (He^*). The negative plate pulsed at -950 V for 30 µs, 60 µs after the leading edge of the nozzle pulse (the other plate was connected with the local ground). The 2^3S_1 state has a lifetime of 7870 s, which is far longer than the $\sim$300 µs flight time to the sample, $\sim$40 cm from the nozzle. The beam was collimated by a skimmer (Beam Dynamics, 3 mm diameter, 2.5° internal angle) placed 12 cm downstream of the nozzle. A fraction of the atoms were ionized by the discharge plates, and these ions (He^+) were removed from the atomic beam with two electrodes. The electrodes were separated by 20 mm, and had a voltage difference of 219 V. The electric field between them

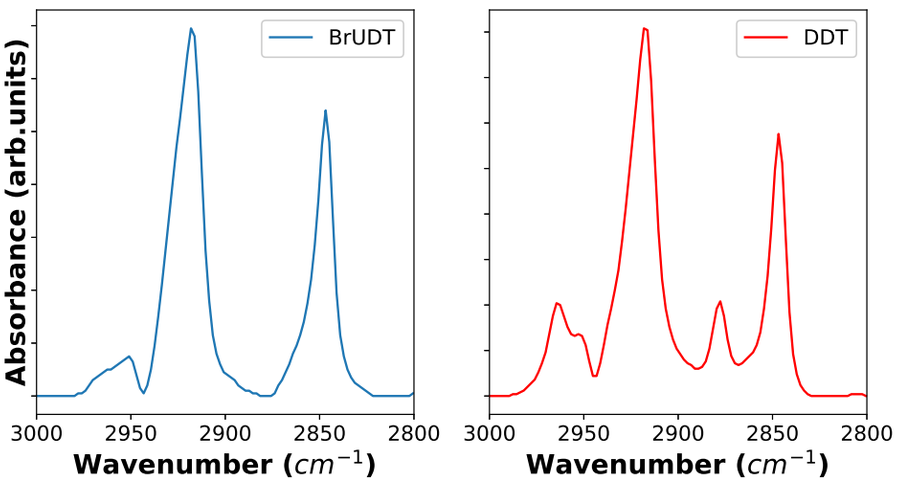

Figure 3. The plots show typical FTIR spectra for the monolayers used in our experiments. The FTIR spectrum of BrUDT is shown in the left panel and the spectrum of DDT is shown in the right panel. Due to the absence of CH_3 in the BrUDT molecules, the peaks associated with CH_3 (2965, 2879 cm^{-1}) are absent in the BrUDT spectrum.

diverted the trajectory of charged particles enough to prevent them from passing through a $3/16$ *in* diameter aperture in a ceramic plate.

The atomic beam was characterized by measuring the electrical current it generated at the sample. Both He^* and He^+ generated a positive current to the sample upon impact.[44] The current signal was filtered with a passive RC filter (2 s lifetime), then fed to a transimpedance amplifier (FEMTO DLPCA-200, bandwidth = 400 kHz, gain = 10^5) to produce a voltage output. A typical voltage trace (fig. 5, panel (a) indicates a small initial current caused by UV photons created at the discharge plates, and then a much larger peak caused by the He^* and He^+.

Given the voltage trace of the larger peak, $V(t)$, the number of electrons which had left the sample, n, is given by

$$n = \frac{1}{e}\int \frac{V(t)}{\text{gain}}\mathrm{d}t\,, \tag{3}$$

where e is the fundamental charge and the gain of the transimpedance amplifier is used. If $He^*$and He^+removed electrons with unit efficiency, this would be equal to the $He^*$and He^+population of the atomic beam. Thus, we can use this estimate as a lower bound. The current traces from 36,000 different nozzle pulses indicates that there were $\geq 3.3(2)\times 10^8$ He^* and He^+ in each pulse.

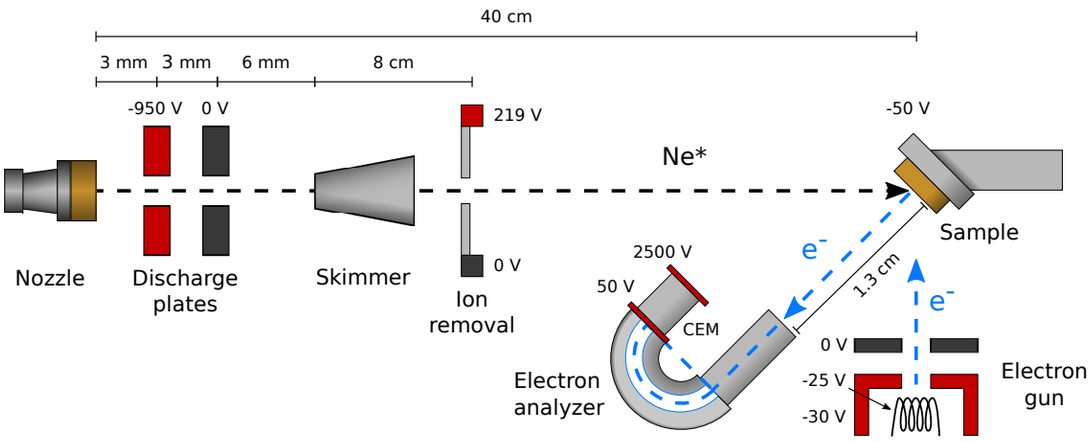

Figure 4. Schematic of the experimental setup. Helium was released from a pulsed nozzle, then excited to a metastable state (He^*) by a pair of discharge plates. The beam was collimated with a skimmer, and ions were removed from the beam with another pair of electrodes and a ceramic plate with an on-axis aperture. When He^* atoms hit the sample, they ejected electrons, which were measured with an electron analyzer. The samples were damaged by a custom-made electron gun.

Plotting the quantity n vs the ion removal voltage (fig. 5 , panel (b)) shows that the ion removal electrodes reduced the fraction of the sample current caused by He^+, and that the fraction was small even when the ion removal was not in use (0 V).

MAES relies on measuring the energy of the electrons ejected by He^* to characterize the SAM. Ejected electrons were repelled from the SAM by biasing the sample at -50 V. Electrons with a certain energy were selected for using a hemispherical electron analyzer (VSW HA 50) set with a pass energy of 4.46 eV, resulting in an energy resolution of 0.27 eV. The population of electrons in that energy class was then measured using a channel electron multiplier (CEM) (Scientific Instrument Services, Detech 206-10). For every pulse of the supersonic nozzle, a different energy class was measured, resulting in a spectrum (e.g. fig. 6). The use of these spectra for diagnosing SAM damage is discussed in section IV.

SAMs were damaged by a low-energy electron beam (30 eV) generated by a simple, custom-built electron-gun. The electron source was a tungsten filament biased at -25 V. The electrons were accelerated towards the SAM by two electrodes, with the first electrode closest to the electron source biased at -30 V and the second electrode biased at 0 V. For each exposure, the electron gun operated for 30 minutes with MAES data taken between each exposure. The electron dosage delivered to the sample in each exposure, $1.91(5)\,\mathrm{C\,cm^{-2}}$, was measured via a picoammeter (Keithley,

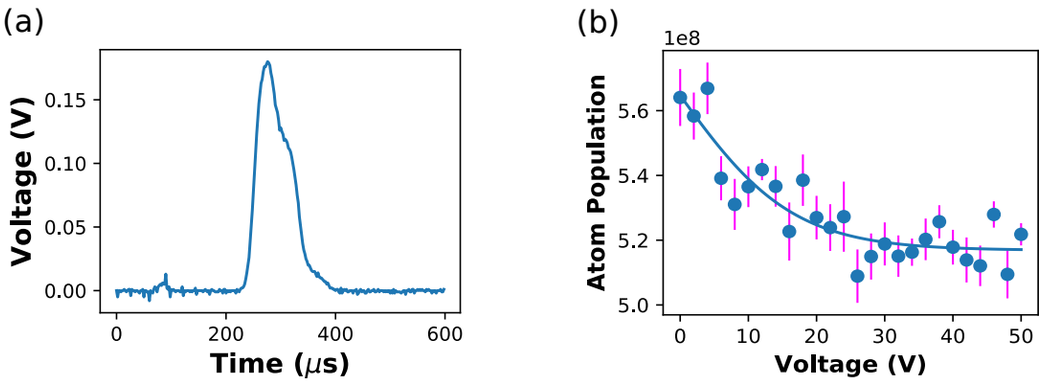

Figure 5. Panel (a) shows the oscilloscope trace for the current due to metastable helium atom (He^*) impact on our sample. The He^* were produced 60 µs after the triggering event and it took on average ∼280 µs to reach the sample. During the electric discharge used to produce He^*, we also created helium ions He^+ and ultraviolet (UV) photons. We excluded the UV emitted electrons using the time difference between the arrival of the UV photons and the He^*. In order to remove the He^+ we used a pair of two electrodes placed before the sample and applied a potential difference between them. This created an electric field transverse to the atomic beam which caused the He^+ to be deflected out of the atomic beam. In panel (b), we show the integrated signal at the sample as a function of the voltage difference applied on the two ion removal electrodes. We can see that with a modest voltage of 50 V the integrated signal approaches an asymptote indicating that most of the ions have been removed. The blue solid line is used as a guide to the eye.

Model 6485) connected between the sample and electrical ground. The average electron energy was determined by measuring the energy of the small fraction of electrons which reflected off of the SAM and into the electron analyzer.

IV. RESULTS

Our first task was to establish that the MAES spectra did not change after repeated probing. This was important in order to ensure that the collected spectra did not significantly change from run to run. This allowed us to average multiple spectra reducing the noise in the data. Moreover, we wanted to validate that metastable atoms were not significantly damaging the sample during the probing process. This was of concern since metastable atoms have been used for lithography purposes.[45,46] However, in both references[45,46] they were able to imprint patterns using continuous beams of metastable atoms for several minutes in juxtaposition with our experiment in which we

used a pulsed beam for the duration of 5 minutes.

In order to address the above concerns we recorded three MAES spectra of a BrUDT sample. As can be seen in fig. 6 the data from each run are almost identical which allowed us to average multiple runs. Furthermore, we confirmed that the samples were not damaged during the probing process. The data points for each spectrum were averaged using a rolling average, where each data point's value was averaged using its closest three neighbors from each side. The first and last three data points from each spectrum are excluded since these data points do not have three neighbors on both of their sides. This intentional data removal does not impact our spectra for two reasons. First, the count rate is virtually constant in those regions, thus we are not losing important information by excluding those regions. Second, the regions excluded have an energy range of 0.075 eV each, which is a negligible portion of the entire spectrum. As a result, we can be confident that there is no significant damage imparted on the sample due to the metastable atoms during the interrogation process.

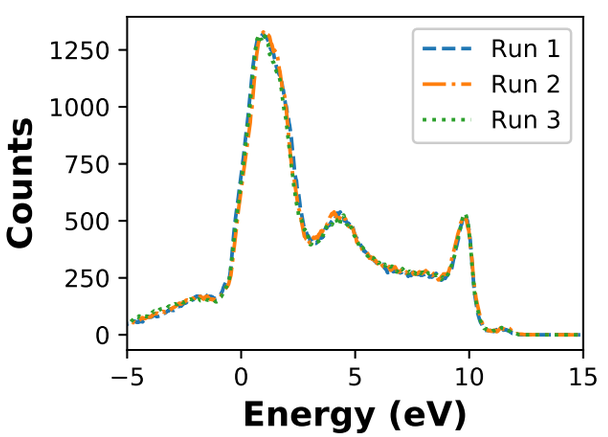

Figure 6. MAES spectra of a BrUDT self-assembled monolayer on a gold coated silicon wafer. Each run lasted for 250 s and our metastable source produced 32.5 µs long pulses at 4 Hz repetition rate. Our sample was biased at −50 V in order to overcome ambient magnetic and electric field by establishing a strong electric field between the sample and the tip of the electron analyzer which is grounded. We can see that the data from each run as well as the average of the three runs overlap significantly giving us confidence that the metastable atoms do not induce damage during the sample's interrogation.

Having established the fact that our beam did not induce significant damage on our samples we then tested our ability to differentiate between self-assembled monolayers made using two

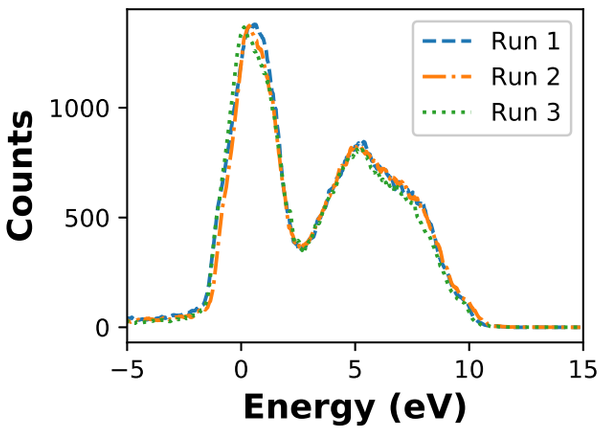

Figure 7. MAES spectra of DDT self-assembled monolayer on gold-coated silicon wafer. We used the same experimental parameters to collect this data with the only difference being that we biased the sample at $-10\,\mathrm{V}$ for these spectra. We can again see that there was minimal variation from run to run and most importantly these spectra do not resemble at all the ones in fig. 6. In these spectra, we again see a prominent narrow peak at $\sim$1 eV and a much broader peak at $\sim$5 eV.

different molecules. For this purpose, we compared samples used in our experiments made with BrUDT molecules against samples made using DDT molecules (fig. 7). Both samples have the same length of carbon chain, namely twelve, as well as the same docking group, the thiolate group. Their only difference is the functional group located at the tail of the chain which is referred to as the tail group. The BrUDT has a bromine tail group (Br) whereas the DDT has a methyl tail group (CH_3). In fig. 7 we show the MAES spectrum for a DDT monolayer. As we can see, the MAES spectra of BrUDT (fig. 6) and DDT (fig. 7) are significantly different with the main difference being the peak located at $\sim$9.5 eV present in the BrUDT spectrum which is absent in the DDT spectrum. Since the only difference between the two molecules is the tail group we attribute this peak to the bromine group. This result confirms that MAES can be used to discriminate between SAMs with different tail groups.

In figs. 6 and 7 we demonstrated that metastable atoms did not degrade the material during the probing process and MAES was able to distinguish different samples. The last and most important part of our project was to expose our sample to an electron beam and monitor the gradual damage of the monolayer. As was mentioned in section III, we exposed the sample 5 times and we delivered $\sim 1.91\,\mathrm{C\,cm^{-2}}$ in each exposure. After each exposure we used MAES to record the

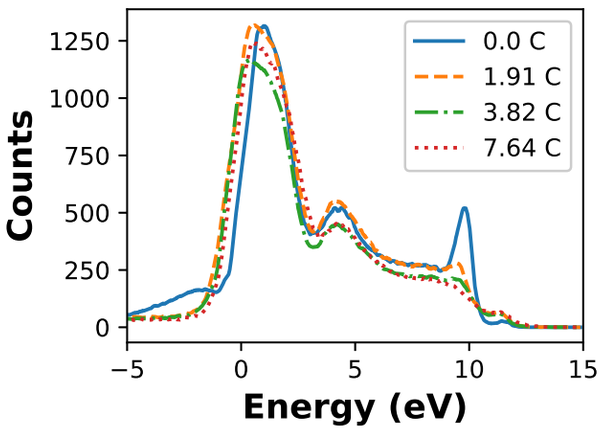

Figure 8. Self-assembled monolayer of BrUDT on gold-coated silicon. This sample was exposed five times to a 30 eV electron beam. Each exposure lasted 30 minutes and delivered $\sim -1.91\,\mathrm{C\,cm^{-2}}$ charge. We can see that after the first exposure the peak located at ∼9.5 eV had significantly diminished with its amplitude reducing after each exposure. The same effect was observed for the peak located at ∼4 eV. The broad shoulder before 0 eV had completely vanished after the first exposure and a smaller peak appeared at ∼11 eV.

electron spectrum of the damaged sample and the spectra are presented in fig. 8. Since MAES is a surface sensitive technique any change in the electron spectra did not have any contribution from the underlying substrate and reflected changes taking place at the SAM. In fig. 8 we can clearly see that the prominent peak at ∼9.5 eV diminished significantly after the first exposure and was completely erased by the end of our experiment. Furthermore, the amplitude of the peak at ∼4 eV decreased with every subsequent electron beam exposure. Lastly we can notice a smaller peak at ∼11 eV was growing with every subsequent exposure. Given our results we conclude that the bromine group was definitely removed from the monolayer since our spectrum after a series of exposures to the electron beam lost its prominent feature at ∼9.5 eV which was the major difference between the BrUDT and the DDT spectra. Intuitively speaking the bromine group is the tail group of the BrUDT molecule making it the most vulnerable to the incoming electrons. However, this is not the only change that happened to the organic monolayer. Due to the other features of the spectrum being modified, we come to believe that other phenomena also took place besides the bromine bond breaking. Based on references,[14,25,27] we suspect that the other features modification are due to cross-linking and chain fragmentation.

V. CONCLUSIONS

In this paper we have presented the use of MAES to monitor damage induced on organic materials in real time. We showed that metastable atoms did not alter our sample during the interrogation process and were able to distinguish two different samples of self-assembled monolayers. The main advantages of using MAES over other techniques are the minimal amount of damage induced on the sample and its ability to probe the surface-most layer of a sample. As a result, using MAES can give us accurate results of what damage was caused on a sample's surface exclusively due to the damaging agent. In our experiment, we were able to clearly see a change in the MAES spectra after an exposure to a low energy electron beam. The MAES spectra of the BrUDT samples lost a prominent peak at $\sim$9.5 eV and were getting broader as the electron exposure increased. Since the peak at $\sim$9.5 eV was absent from the DDT spectra we attributed that peak to the bromine tail group of the BrUDT. For this reason, we believe that during each electron exposure there was a bond breaking event between the bromine tail group and the rest of the molecule. Besides the bromine bond breaking, we see a general change in our MAES spectra which we attribute to cross-linking and chain fragmentation.

DATA AVAILABILITY

The data that support the findings of this study are available from the corresponding author upon reasonable request.

ACKNOWLEDGMENTS

This research project was funded in part by The Welch Foundation under grants no. F-1258 and no. F-1722, and by the National Science Foundation (NSF) under grants no. PHY 1704059 and no. CHE-1807215.

REFERENCES

[1]I. Baccarelli, I. Bald, F. A. Gianturco, E. Illenberger, and J. Kopyra, Phys. Rep. **508**, 1 (2011).

[2]J. H. Hoeijmakers, N. Engl. J. Med. **361**, 1475 (2009).

[3]P. Bandelier, A.-L. Charley, and A. Lagrange, in *Lithography* (ISTE Ltd and John Wiley & Sons, Inc., 2011) pp. 1–40.

[4]H. J. Levinson, in *Principles of Lithography* (SPIE Press, 2011) third edition ed., pp. 51–108.

[5]C. G. Pantano, A. S. D'Souza, and A. M. Then, in *Beam Effects, Surface Topography, and Depth Profiling in Surface Analysis*, Vol. 5, edited by A. W. Czanderna, T. E. Madey, and C. J. Powell (Kluwer Academic Publishers, Boston, 2002) pp. 39–96.

[6]J. H. Thomas, in *Beam Effects, Surface Topography, and Depth Profiling in Surface Analysis*, edited by A. W. Czanderna, T. E. Madey, and C. J. Powell (Springer US, Boston, MA, 2002) pp. 1–37.

[7]R. Egerton, P. Li, and M. Malac, Micron **35**, 399 (2004).

[8]K. R. Vinothkumar and R. Henderson, Quart. Rev. Biophys. **49**, e13 (2016).

[9]P. E. Laibinis, G. M. Whitesides, D. L. Allara, Y. T. Tao, A. N. Parikh, and R. G. Nuzzo, J. Am. Chem. Soc. **113**, 7152 (1991).

[10]A. Ulman, Chem. Rev. **96**, 1533 (1996).

[11]C. L. McGuiness, G. A. Diehl, D. Blasini, D.-M. Smilgies, M. Zhu, N. Samarth, T. Weidner, N. Ballav, M. Zharnikov, and D. L. Allara, ACS Nano **4**, 3447 (2010).

[12]J. M. MacLeod and F. Rosei, Small **10**, 1038 (2014).

[13]J. C. Love, L. A. Estroff, J. K. Kriebel, R. G. Nuzzo, and G. M. Whitesides, Chem. Rev. **105**, 1103 (2005).

[14]W. Geyer, V. Stadler, W. Eck, M. Zharnikov, A. Gölzhäuser, and M. Grunze, Appl. Phys. Lett. **75**, 2401 (1999).

[15]C. Zhou, A. Trionfi, J. W. P. Hsu, and A. V. Walker, J. Phys. Chem. C **114**, 9362 (2010).

[16]I. F. Gallardo and L. J. Webb, Langmuir **28**, 3510 (2012).

[17]N. Afsharimani, B. Uluutku, V. Saygin, and M. Z. Baykara, J. Phys. Chem. C **122**, 474 (2018).

[18]T. Zhang, Z. Cheng, Y. Wang, Z. Li, C. Wang, Y. Li, and Y. Fang, Nano Lett. **10**, 4738 (2010).

[19]M. D. Porter, T. B. Bright, D. L. Allara, and C. E. D. Chidsey, J. Am. Chem. Soc. **109**, 3559 (1987).

[20]S. Chenakin, B. Heinz, and H. Morgner, Surf. Sci. **397**, 84 (1998).

[21]Q. Guo and F. Li, Phys. Chem. Chem. Phys. **16**, 19074 (2014).

[22]W. A. Fies, J. W. Dugger, J. E. Dick, L. M. Wilder, K. L. Browning, M. Doucet, J. F. Browning, and L. J. Webb, Langmuir **35**, 5647 (2019).

[23]J. M. Holton, J. Synchrotron Radiat. **16**, 133 (2009).

[24]M. F. Lavin, A. Jenkins, and C. Kidson, J. Bacteriol. **126**, 6 (1976).

[25]K. Heister, M. Zharnikov, M. Grunze, L. S. O. Johansson, and A. Ulman, Langmuir **17**, 8 (2001).

[26]T. Laiho, J. Leiro, and J. Lukkari, Appl. Surf. Sci. **212-213**, 525 (2003).

[27]H. U. Müller, M. Zharnikov, B. Völkel, A. Schertel, P. Harder, and M. Grunze, J. Phys. Chem. B **102**, 7949 (1998).

[28]M. Zharnikov, W. Geyer, A. Gölzhäuser, S. Frey, and M. Grunze, Phys. Chem. Chem. Phys. **1**, 3163 (1999).

[29]C. Yildirim, M. Fu, A. Terfort, and M. Zharnikov, J. Phys. Chem. C **121**, 567 (2017).

[30]M. Schmid, X. Wan, A. Asyuda, and M. Zharnikov, J. Phys. Chem. C **123**, 28301 (2019).

[31]C. Neumann, R. A. Wilhelm, M. Küllmer, and A. Turchanin, Faraday Discuss. , 10.1039/C9FD00119K (2020).

[32]B. Heinz and H. Morgner, Surf. Sci. **372**, 100 (1997).

[33]S. S. Hodgman, R. G. Dall, L. J. Byron, K. G. H. Baldwin, S. J. Buckman, and A. G. Truscott, Phys. Rev. Lett. **103**, 053002 (2009).

[34]H. Conrad, G. Doyen, G. Ertl, J. Küppers, W. Sesselmann, and H. Haberland, Chem. Phys. Lett. **88**, 281 (1982).

[35]Y. Harada, S. Masuda, and H. Ozaki, Chem. Rev. **97**, 1897 (1997).

[36]H. Morgner, in *Advances in Atomic, Molecular, and Optical Physics*, Advances in Atomic, Molecular, and Optical Physics, Vol. 42 (Academic Press, 2000) pp. 387–483.

[37]H. D. Hagstrum, Physical Review **96**, 336 (1954).

[38]H. D. Hagstrum, Physical Review **150**, 495 (1966).

[39]H. D. Hagstrum, in *Electron and Ion Spectroscopy of Solids*, NATO Advance Study Institutes Series, Vol. 32 (Plenum Press, 1978).

[40]H. D. Hagstrum, Physical Review Letters **43**, 1050 (1979).

[41]H. Hotop, in *Atomic, Molecular, and Optical Physics: Atoms and Molecules*, Experimental Methods in the Physical Sciences, Vol. 29B (Academic Press, 1996) pp. 191–215.

[42]I. F. Gallardo and L. J. Webb, Langmuir **26**, 18959 (2010).

[43]J. P. Collman, N. K. Devaraj, and C. E. D. Chidsey, Langmuir **20**, 1051 (2004).

[44]Excited states besides He^* would also cause a current, but their lifetime is too short for them to reach the sample before de-excitation to the ground state.

[45]A. Bard, K. K. Berggren, J. L. Wilbur, J. D. Gillaspy, S. L. Rolston, J. J. McClelland, W. D. Phillips, M. Prentiss, and G. M. Whitesides, J. Vac. Sci. Technol. B **15**, 1805 (1997).

[46]S. Nowak, T. Pfau, and J. Mlynek, Microelectron. Eng. **35**, 427 (1997).

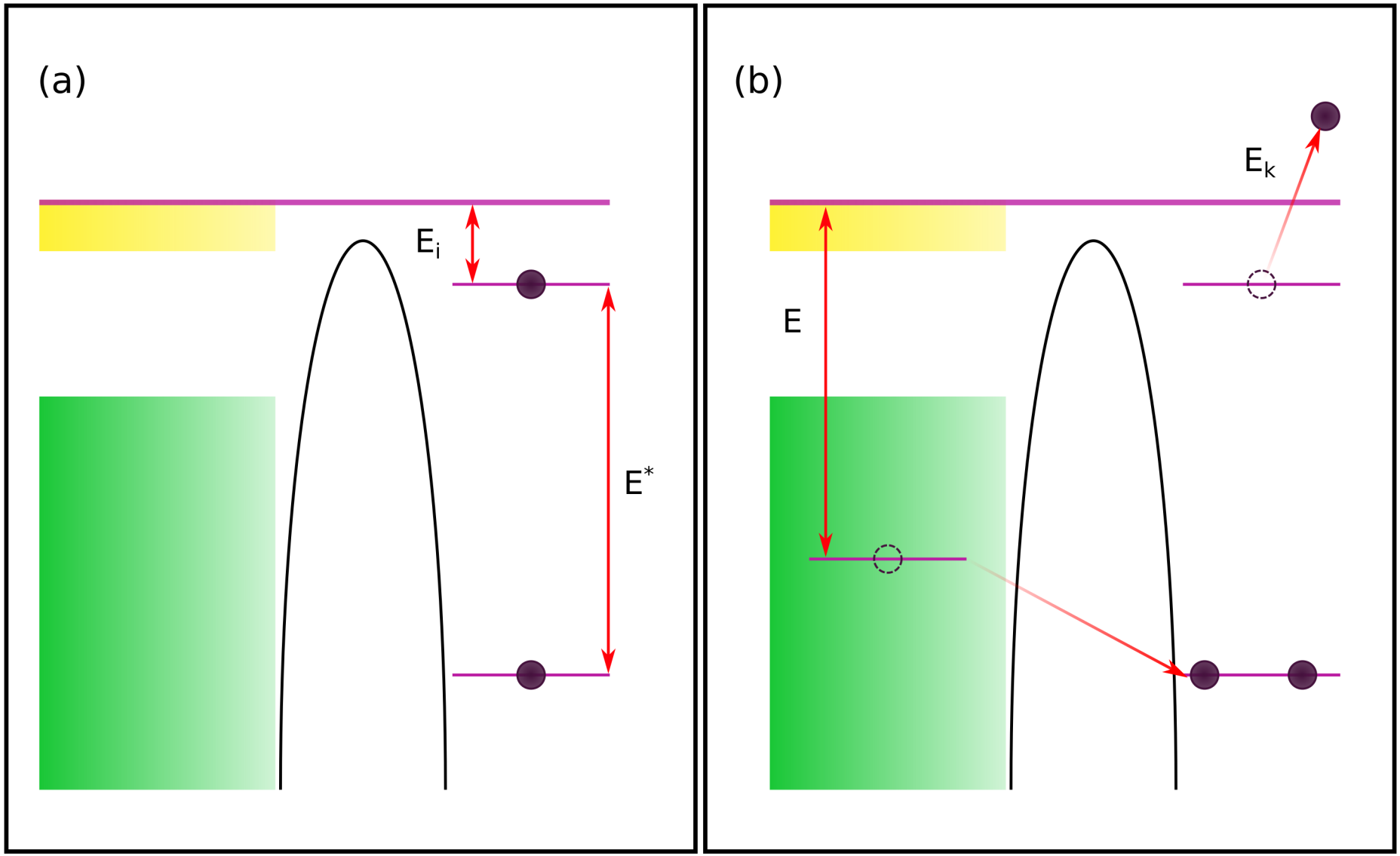
(a)
E_i
E^*
(b)
E_k
E

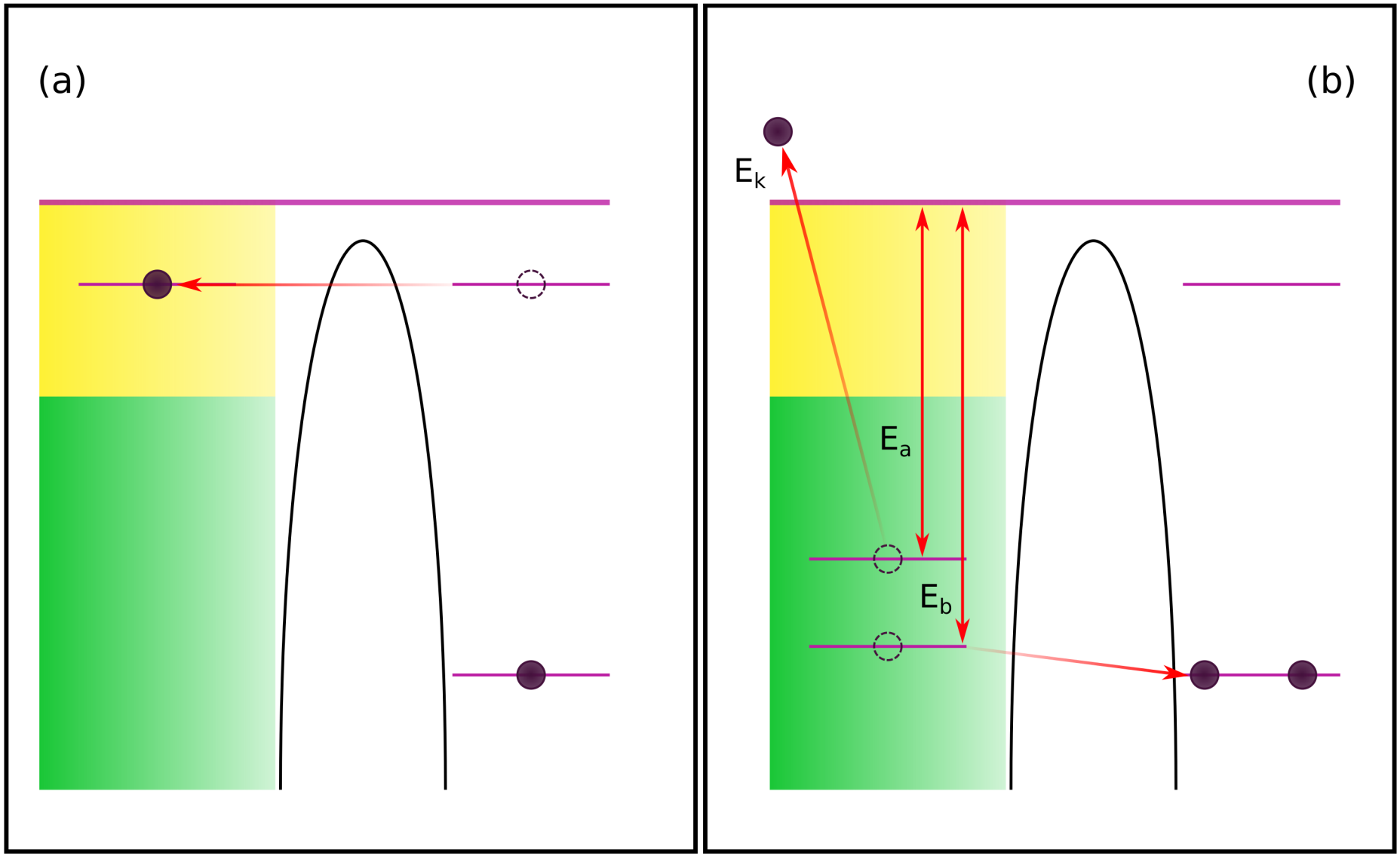
(a)
(b)
E_k
E_a
E_b

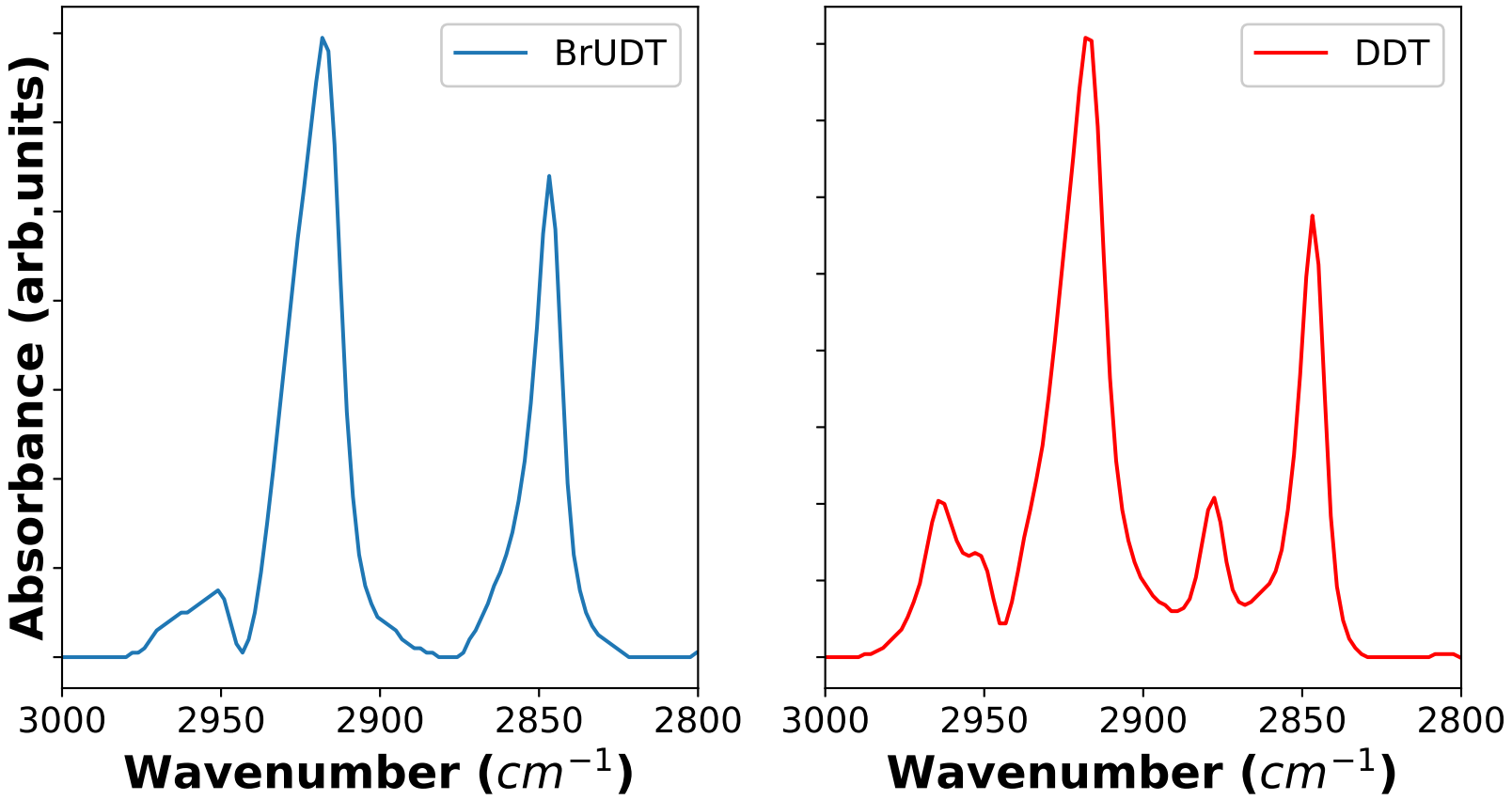
BrUDT
DDT
Absorbance (arb.units)
3000
2950
2900
2850
2800
Wavenumber (cm^{-1})
3000
2950
2900
2850
2800
Wavenumber (cm^{-1})

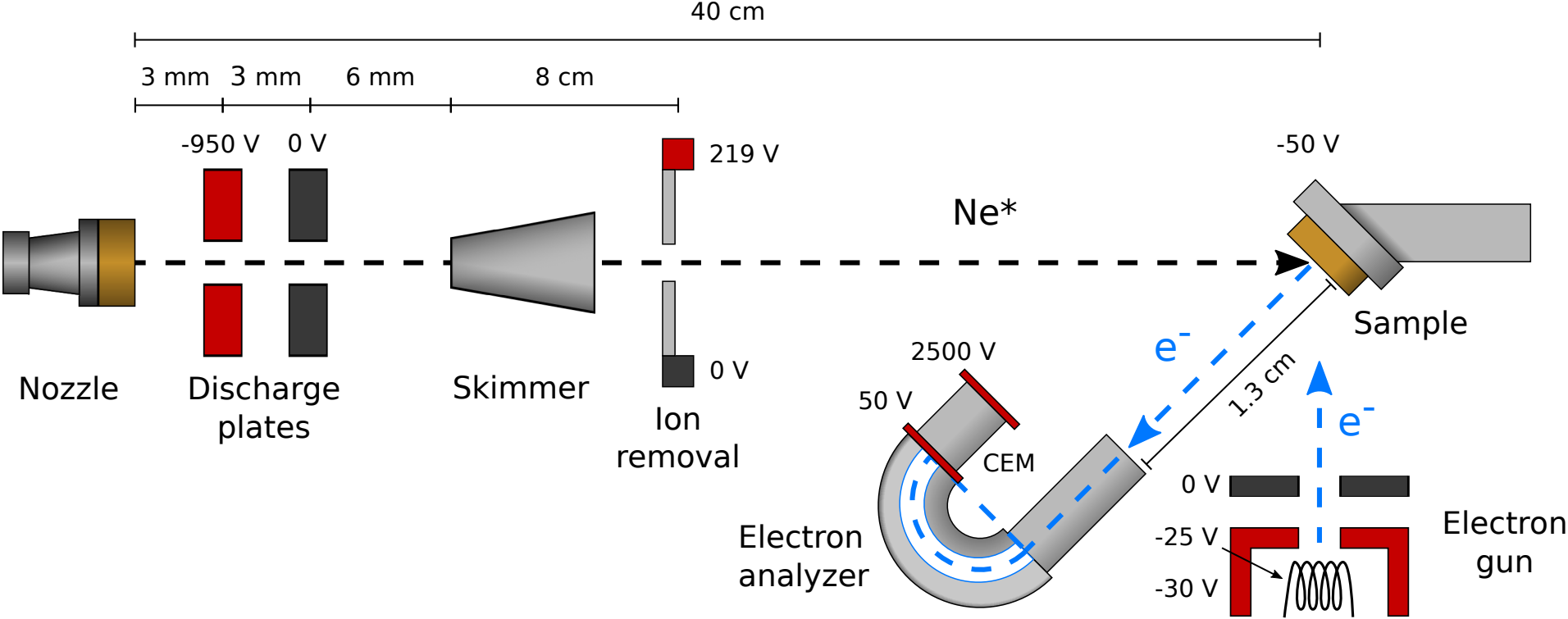
40 cm
3 mm
3 mm
6 mm
8 cm
-950 V
0 V
219 V
0 V
-50 V
Ne*
Nozzle
Discharge plates
Skimmer
Ion removal
Sample
2500 V
50 V
CEM
e⁻
1.3 cm
e⁻
0 V
-25 V
-30 V
Electron analyzer
Electron gun

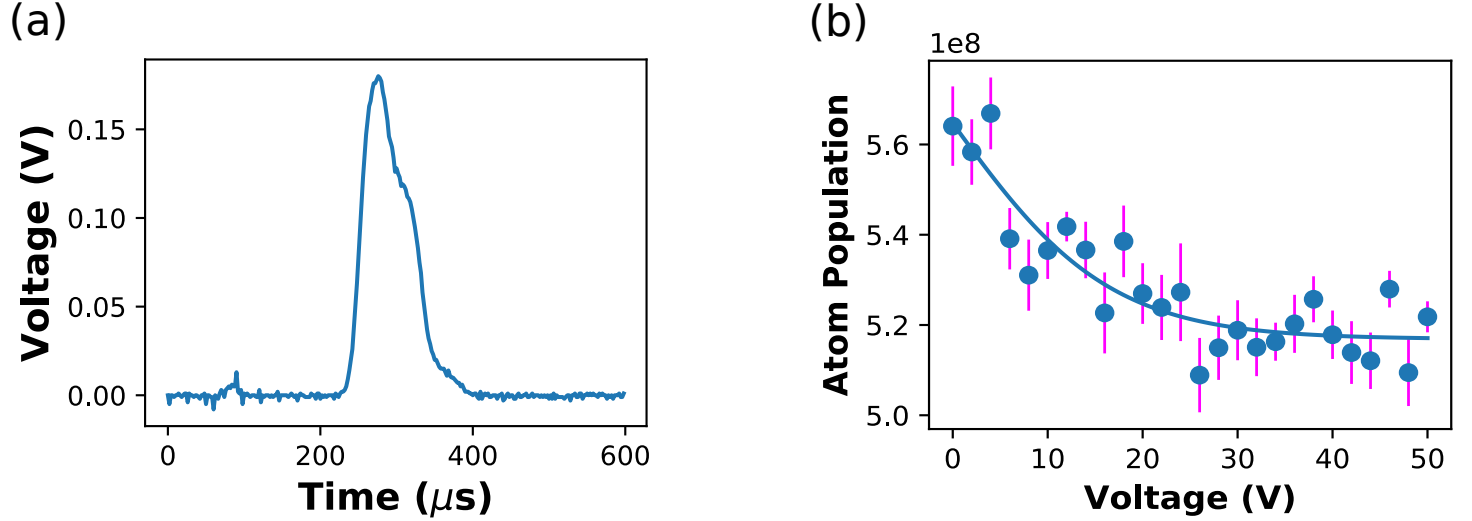
(a)
Voltage (V)
0.15
0.10
0.05
0.00
0
200
400
600
Time (μs)
(b)
1e8
Atom Population
5.6
5.4
5.2
5.0
0
10
20
30
40
50
Voltage (V)

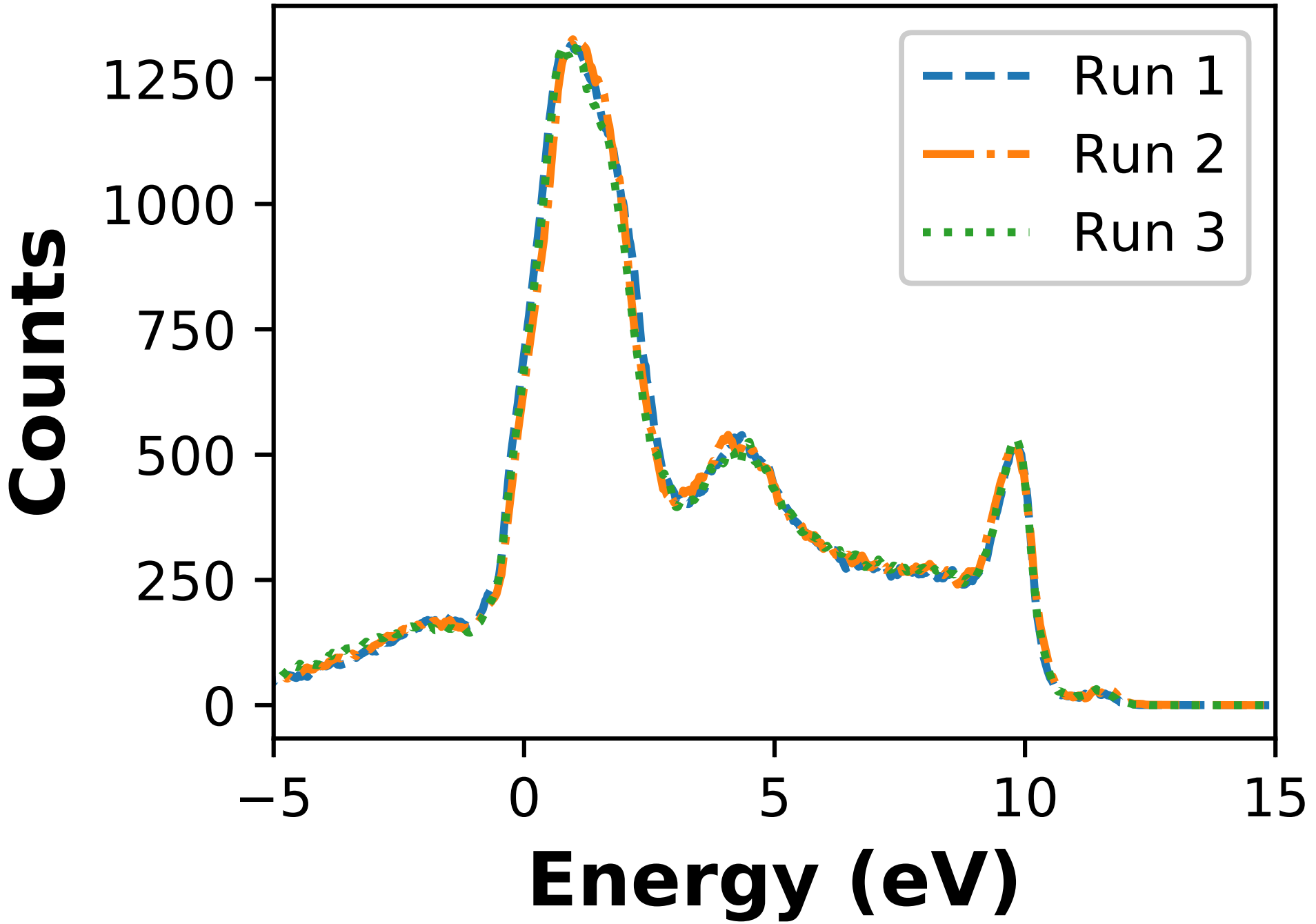
Run 1
Run 2
Run 3
Counts
1250
1000
750
500
250
0
−5
0
5
10
15
Energy (eV)

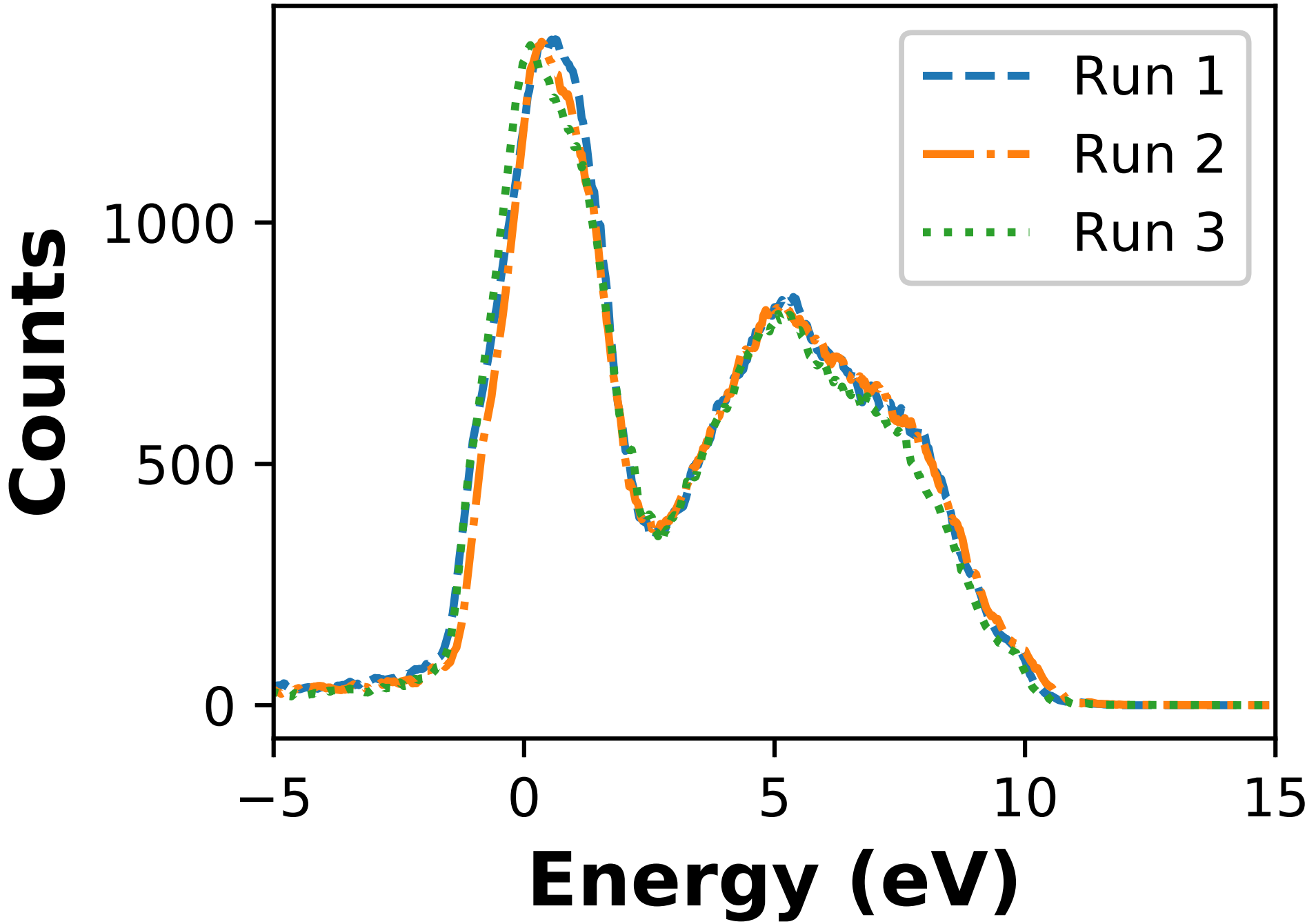
Run 1
Run 2
Run 3
Counts
1000
500
0
−5
0
5
10
15
Energy (eV)

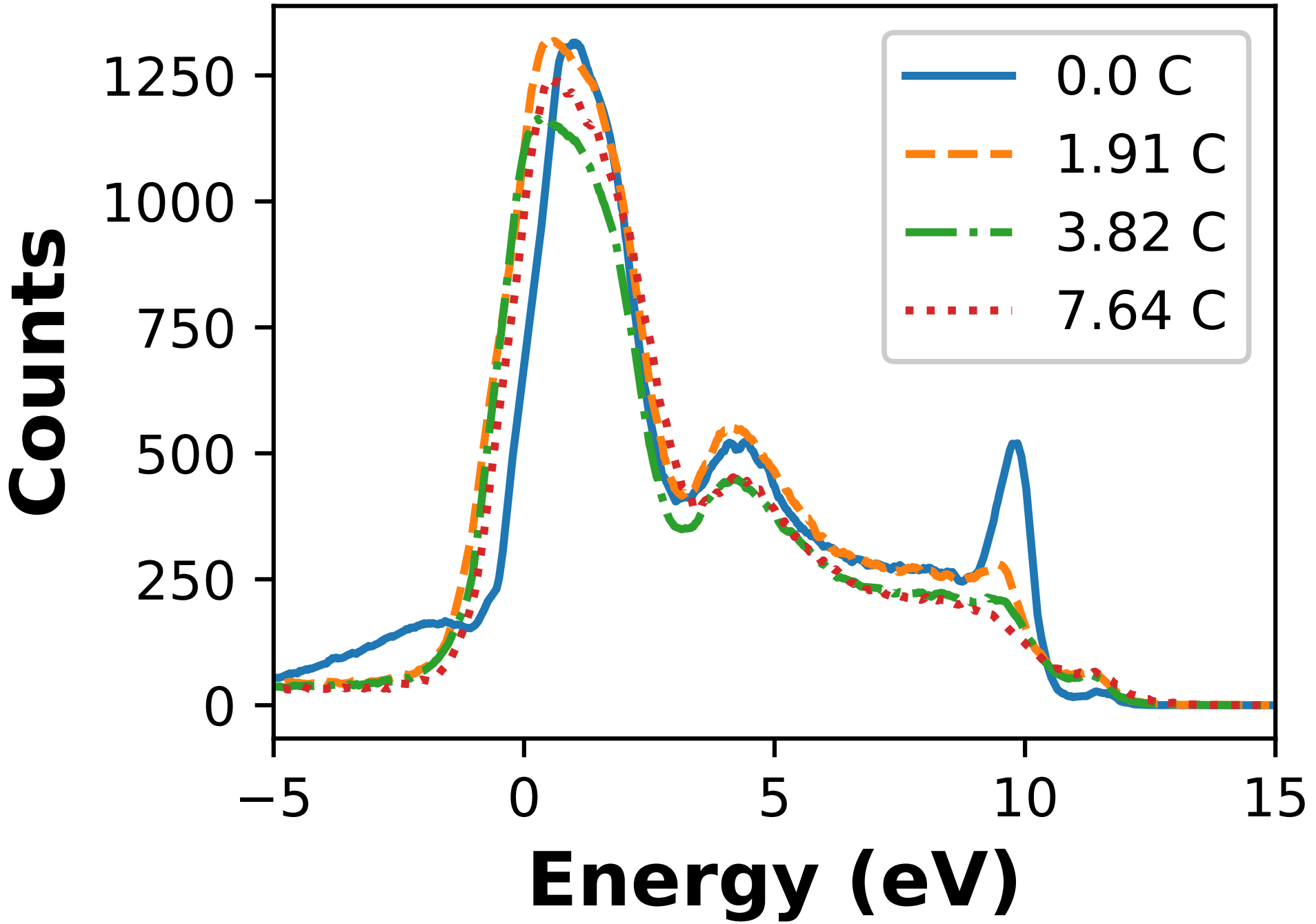
0.0 C
1.91 C
3.82 C
7.64 C
Counts
1250
1000
750
500
250
0
−5
0
5
10
15
Energy (eV)